Optoacoustic classification of diabetes mellitus with the synthetic impacts via optimized neural networks

Tao Liu [a], Zhong Ren [a,b,*], Chengxin Xiong [a], Wenping Peng [a], Junli Wu [a], Shuanggen Huang [c,**], Gaoqiang Liang [a], Bingheng Sun [a]

[a] *Key Laboratory of Optic-electronic and Communication, Jiangxi Science and Technology Normal University, 330038 Nanchang, Jiangxi, China*
[b] *Key Laboratory of Optic-electronic Detection and Information Processing of Nanchang City, Jiangxi Science and Technology Normal University, 330038 Nanchang, Jiangxi, China*
[c] *Agricultural Equipment Key Laboratory of Jiangxi Provincial, Jiangxi Agriculture University, 330045 Nanchang, Jiangxi, China*

ARTICLE INFO

ABSTRACT

A highly accurate classification of diabetes mellitus (DM) with the synthetic impacts of several variables is first studied via optoacoustic technology in this work. For this purpose, an optoacoustic measurement apparatus of blood glucose is built, and the optoacoustic signals and peak–peak values for 625 cases of *in vitro* rabbit blood are obtained. The results show that although the single impact of five variables are obtained, the precise classification of DM is limited because of the synthetic impacts. Based on clinical standards, different levels of blood glucose corresponding to hypoglycaemia, normal, slight diabetes, moderate diabetes and severe diabetes are employed. Then, a wavelet neural network (WNN) is utilized to establish a classification model of DM severity. The classification accuracy is 94.4 % for the testing blood samples. To enhance the classification accuracy, particle swarm optimization (PSO) and quantum-behaved particle swarm optimization (QPSO) are successively utilized to optimize WNN, and accuracy is enhanced to 98.4 % and 100 %, respectively. It is demonstrated from comparison between several algorithms that optoacoustic technology united with the QPSO-optimized WNN algorithm can achieve precise classification of DM with synthetic impacts.

1. Introduction

As a chronic and global disease, diabetes mellitus (DM) has seriously been affecting human life and health. At present, DM cannot be completely cured, and it can only be controlled by hypoglycaemic drugs. The precise measurement of blood glucose values (BGVs) or the assessment of severity are important steps during the control of DM. In clinics, the traditional monitoring of DM involves collecting blood by puncturing the skin tissue, and then it is analyzed by a biochemical analyzer. As the destructive way has the risk of secondary infection, nondestructive methods will be the future trend. To date, there have been some reports on nondestructive blood glucose detection, for example, electrochemical [1], metabolic thermal integration [2], impedance [3] and reverse ion [4]. As some non-optical methods have a certain irritant effect on human skin, optical approaches have already become a research hotspot in

---

* Corresponding authorKey Laboratory of Optic-electronic and Communication, Jiangxi Science and Technology Normal University, 330038 Nanchang, Jiangxi, China.
** Corresponding author.
E-mail addresses: renzhong0921@163.com (Z. Ren), 45940718@qq.com (S. Huang).

nondestructive blood glucose measurement.

There are some optical technologies are used to measure blood glucose [5–13]. For these purely optics, the spectra will be affected by the scattering light in human skin, similar to a chaotic medium. Among the nondestructive technologies, optoacoustic (or photoacoustic) spectroscopy [14–16] is a rapidly developing and promising detection technology. Compared with optical methods, optoacoustic technology has higher precision because the captured signals are ultrasonic waves rather than photons. Moreover, the decay of ultrasonic waves is weaker than that of photons in human skin. Optoacoustic technology not only retains the advantages of high sensitivity and contrast of optical methods but also solves the attenuation problem of signal propagation in human tissues.

To date, some scholars have already conducted studies on the optoacoustic monitoring of blood glucose [17–19]. Namita et al. [20] monitored glucose solutions and horse blood via NIR laser-induced ultrasound. Gao et al. [21] used the fusion method of optoacoustic peak–peak value and peak decay time to perform optoacoustic experiments of glucose solutions. Shen and Lu [22] utilized optoacoustic technology to perform blood glucose detection research. Zhang [23] developed a portable optoacoustic detection device suitable for nursing and achieved *in vitro* optoacoustic detection of trace 20 μL blood at a wavelength of 520 nm. Srivastava [24] used the modulated optoacoustic technique to detect human blood plasma mixed intralipid phantoms *in vitro*. Tsai et al. [25] studied biochemical blood parameters by using optoacoustic absorption spectroscopy. Long et al. [26] built a simulation optoacoustic model considered human skin, blood and detector limitation, and employed Teager-Kaiser main energy method to eliminate the interference of noise and medium. Ahn et al. [27] performed the optoacoustic *in vivo* monitoring for the growth of animals blood vessels based on the change of blood glucose. Yang [28] developed a optoacoustic multi-spectral measurement system to detect the aqueous glucose, and the machine learning was utilized to predict the glucose concentration. Yang [29] performed optoacoustic measurement glucose solution at 1535 nm and explore the impact of BGV on optoacoustic signal. In addition, the optoacoustic detection of blood glucose in the mid-infrared wavebands was also reported [30,31].

However, the measurement of DM will be inevitably impacted by some elements in practice. There have been few studies on the impacting of blood glucose on optoacoustic measurements in recent years. Tao et al. [32] investigated the sensitivity of optoacoustic signals to temperature in glucose solutions. It was found that the temperature increased linearly with laser energy. Tanaka [33] also explored the relationship between optoacoustic value and temperature, as well as light intensities. Zhao [34] verified that the influences of optoacoustic glucose measurement include physiological and temperatures, as well as skin heterogeneity. Zhao and Tao [35] explored the influences of temperature and the compressibility of glucose solution on the optoacoustic measurement of BGVs. Ren et al. [36,37] studied the impacts of other blood components on the optoacoustic monitoring of BGVs. Christina et al. [38] investigated the elements of impacting the blood glucose measurement including ambient conditions, hardware system and operation errors.

Although the variables impacting the optoacoustic measurement of blood glucose have already been explored by a few researchers, there are still many impacting variables that need to be further explored and expanded. Moreover, to date, the synthetic impacts of several variables on the optoacoustic measurement of DM have not been systematically explored worldwide. Additionally, the research on optoacoustic measurement of blood glucose has mainly focused on the *in vitro* or *in vivo* quantitative measurement of BGV in recent years [39–43]. For the treatment and control of DM, precise qualitative classification and assessment of the severity is very important and necessary under the synthetic impacts of several variables. However, the optoacoustic qualitative classification of DM with the synthetic impacts of several variables has not been studied worldwide. In this work, the qualitative classification of DM with the synthetic impacts of several variables was first investigated using optoacoustic technology united with the optimized wavelet neural network (WNN) method. As a kind of artificial neural network (ANN), WNN [44] is not only an ANN algorithm on the basis of wavelet theory but also a fusion of wavelet transform and ANN [45].

There are three purposes in this work. The first is to build an optoacoustic monitoring equipment to realize the optoacoustic classification of DM with the synthetic impacts of several variables (temperature, energy absorption, BGV, detection distance and flow rate). The second is to accomplish a precise qualitative classification of DM with synthetic impacts by using the WNN algorithm according to clinical medical standards. The third is to enhance the qualitative classification accuracy of DM using the PSO [46,47] and QPSO [48] optimized WNN algorithms.

2. Theories

2.1. Optoacoustic theory

The theories of optoacoustic technology are the effect of photoinduced ultrasonication and the thermoelastic mechanism [49]. Although the optoacoustic mechanism is represented via the wave equation [50], a semiempirical formula [51] given in *Eq.*(1) can be generally employed to describe the optoacoustic signal, i.e.,

$$p = k\frac{E\mu_\alpha\beta v^n}{C_p r^m R^l} \tag{1}$$

where μ_α denotes the absorbance coefficient of the detected substance. E denotes the laser's irradiation energy. β denotes the thermal expansion index. C_p denotes the specific heat volume. r denotes the detection distance. R denotes the optoacoustic effective radius. k is the scaling coefficient.

2.2. Classification modeling

WNN [52,53] was selected to conduct qualitative classification of BGV with the synthetic impacts of several variables in here. In the WNN, five impacting variables, i.e., temperature, energy absorption, flow rate, detection distance and peak–peak value, were utilized as the input data, which were weighted and summed. Then, the wavelet transform was adopted to carry out the translation and scaling operations.

Fig. 1 is the structural diagram of WNN.

In Fig. 1, $X = [x_1^g, x_2^g, …, x_p^g]$ are p input data, where the superscript g is the index of G groups of input data ($g = 1,2, …, G$). In hidden layer, a Morlet wavelet function [54] given in $Eq.(2)$ was constructed as the excitation function:

$$\overset{i}{f}(x) = e^{-\frac{x^2}{2}} * \cos(1.75x) \tag{2}$$

The output value (O_k^g) of hidden layer is expressed as $Eq.(3)$

$$O_k^g = \overset{k}{f}\left(\frac{\sum\limits_{p=1}^{P} \omega_{kp} x_p^g - b}{a} \right) \tag{3}$$

where ω_{kp} denotes the weight values connecting input with hidden layers. a denotes the scaling variable of the excitation function, and b denotes the translation variable of the excitation function in $Eq.(2)$.

The output value y_j^g of WNN can be given in $Eq.(4)$:

$$y_j^g = \overset{'}{h}\left(\sum_{k=1}^{K} \omega_{jk} O_k^g \right) \tag{4}$$

where ω_{jk} denotes the weight values connecting hidden with output layers. $h^{'}(\bullet)$ denotes Sigmoid function.

Assuming the anticipated output is d_j^g, the training target error function is expressed in $Eq.(5)$:

$$E_j^g = \frac{1}{2G} \sum_{g=1}^{G} \sum_{j=1}^{J} \left(d_j^g - y_j^g \right) \tag{5}$$

Additionally, two groups of weight values (ω_{kg} and ω_{jk}), and scaling variable (a) and translation variable (b) of wavelet excitation function should be adjusted by using error back propagation, which are given in $Eqs.(6)$:
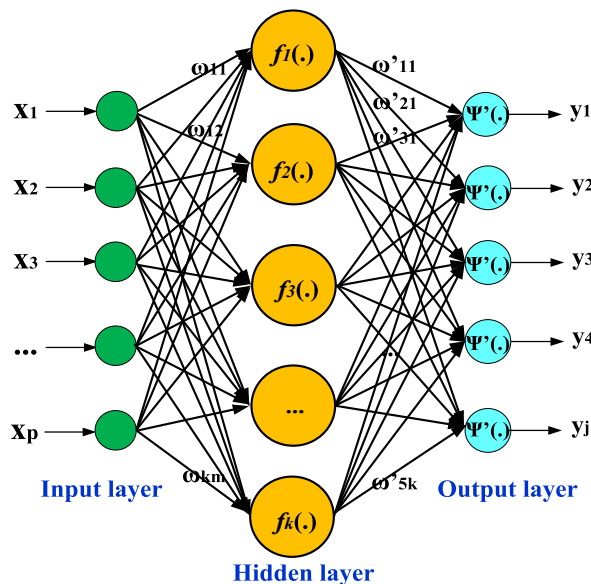
Fig. 1. WNN algorithm.

$$\begin{cases} \omega_{jk}^{new} = \omega_{jk}^{old} + \eta \sum_{k=1}^{K} \dfrac{\partial E_j^g}{\partial \omega_{jk}} \\[2ex] \omega_{kg}^{new} = \omega_{kg}^{old} + \eta \sum_{g=1}^{G} \dfrac{\partial E_j^g}{\partial \omega_{kg}} \\[2ex] a^{up} = a^{ori} + \lambda \sum_{g=1}^{G} \dfrac{\partial E_j^g}{\partial a} \\[2ex] b^{up} = b^{ori} + \lambda \sum_{g=1}^{G} \dfrac{\partial E_j^g}{\partial b} \end{cases} \tag{6}$$

where ω_{jk}^{new}, ω_{kg}^{new}, a^{up} and b^{up} are the adjusted weight values, the scaling and the translation variables of wavelet excitation function, respectively. ω_{jk}^{old}, ω_{kg}^{old}, a^{ori} and b^{ori} are the original weight values, the scaling variable and translation variable, respectively. η and λ denote the learning rates.

2.3. Optimization method

Because PSO has the tendency to drop into the local optimum and generate the oscillation phenomenon [55], a QPSO algorithm [56,57] was utilized to optimize the WNN in this study. Fig. 2 presents the QPSO-WNN method.

In QPSO, the positions of particles should be updated according to *Eqs.*(7):
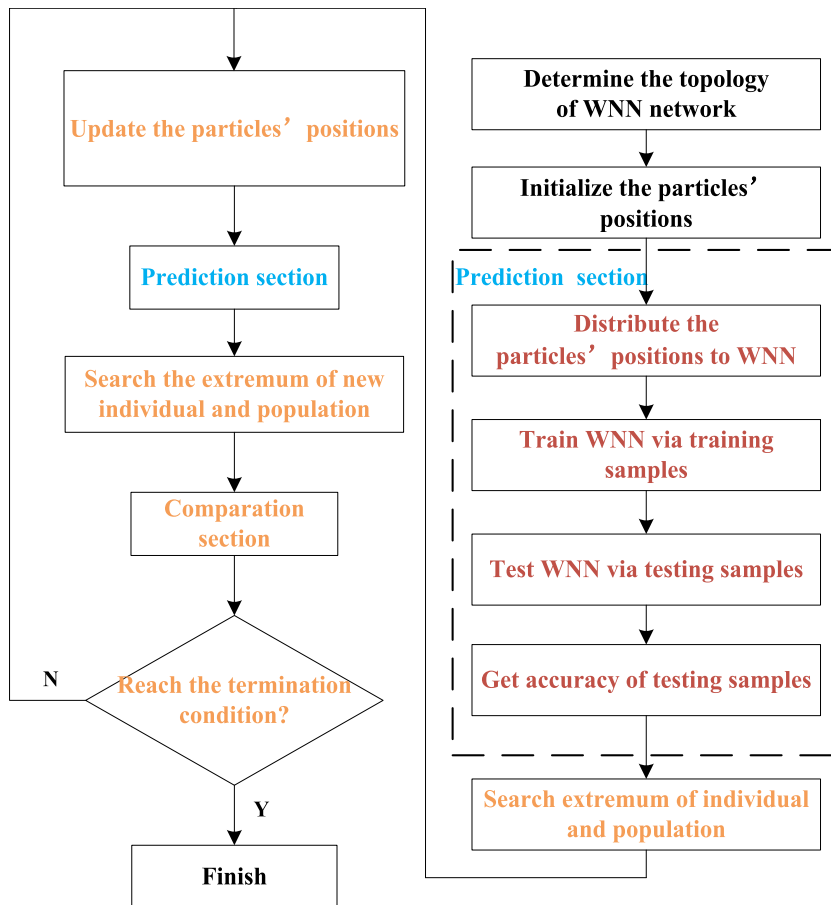
Fig. 2. QPSO-WNN method.

$$\begin{cases} \varphi = \psi \times G_{best} + (1 - \psi) \times Z_{best} \\ pp(n + 1) = \varphi \pm \alpha \times |P_{best} - pp(n)| \times \ln\left(\dfrac{1}{u}\right) \end{cases} \tag{7}$$

In Eq. (7), G_{best} denotes individual extreme. Z_{best} denotes group extreme. φ is the local attraction factor. α ($0 < \alpha < 1$) is the coefficient of shrinkage-expansion employed to control convergent speed. ψ and u are random numbers, $\psi, u \in (0, 1)$. For the symbol "$\pm$", the probability of positive or negative is 50 %, which enhances the randomness of particle. P_{best} is the average optimum of particles, which can be expressed in *Eq.*(8):

$$P_{best} = \frac{1}{K} \sum_{j=1}^{K} G_{bestj} \tag{8}$$

In Eq. (8), K is the total number of particles. The individual and group extremes should be updated based on the following formula:
For individual extremes,

$$G_{best}(n) = \begin{cases} pp(n) \text{ when } f(pp(n)) > f(G_{best}(n-1)) \\ G_{best}(n-1) \text{ when } f(pp(n)) \le f(G_{best}(n-1)) \end{cases} \tag{9}$$

For group extremes,

$$Z_{best}(n) = \begin{cases} pp(n) \text{ when } f(pp(n)) > f(Z_{best}(n-1)) \\ Z_{best}(n-1) \text{ when} f(pp(n)) \le f(Z_{best}(n-1)) \end{cases} \tag{10}$$

According to *Eqs.* (9) and (10), QPSO is superior to PSO in terms of a simpler evolutionary equation, fewer adjusting parameters, and faster convergence [58].

3. Experimental methods

3.1. Equipment

To obtain the optoacoustic signals and peak–peak values of blood with various BGVs, an experimental equipment of blood glucose optoacoustic measurement was built (Fig. 3(a)).

As shown in Fig. 3(a), after a pulsed laser beam was excited from a wavelength-tunable pulse laser (OPOlette™ 532II, OPOTEK), the laser beam passes through three reflectors, a diaphragm and a focus lens, then the focal spot drops in the whole blood sample which flows in the inner cavity of the silicone microtubule. Due to the effect of photoinduced ultrasonication, the whole blood irradiated by the focal spot will generate optoacoustic signals, and the optoacoustic signals were received by a focus-typed ultrasonic sensor (2.5C14SJ50XJ) with 2.5 MHz placed directly under a section of silicone microtubule. After the ultrasonic sensor transformed the optoacoustic intensity information into analogue voltage signals, an analog amplifier (ATA-5620, Aigtek, Xi'an, China) was utilized to amplify the signals, and an analog filter (type: BLP-7-50+) was utilized for denoising. Then, a dual-trance digital oscilloscope (54642D, Agilent) was utilized to acquire the preprocessed signals and convert them to digital signals. To achieve signal acquisition, the pulse trigger signal of the pulse laser was connected with one input channel of the digital oscilloscope to be utilized as synchronous trigger. A
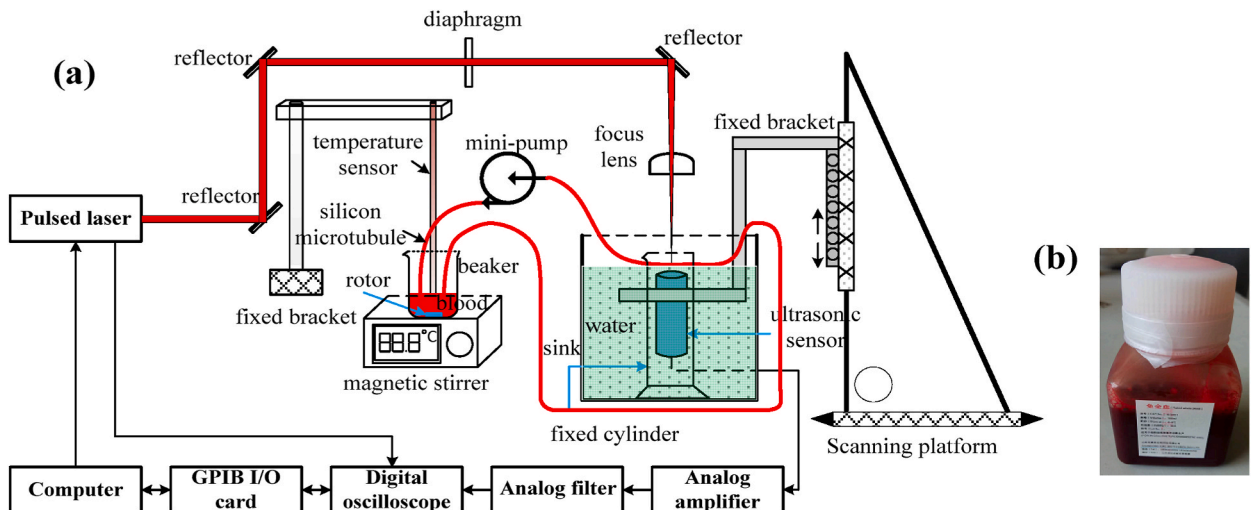
Fig. 3. The blood glucose optoacoustic measurement experimental equipment (a), and a rabbit whole blood sample (b).

data transmission card in GPIB-USB mode was employed to transfer the blood glucose optoacoustic data. The custom signal acquisition and controlling program was performed by LabVIEW software.

In addition, to imitate blood flow in human body and change blood samples, a custom-built cycling apparatus was built. It comprised a mini water pump, silicone microtubules, a beaker and a temperature controller. To explore the impact of the blood flow rate, flow rates of blood samples can be changed by the different rotational speeds of water pump. In general, the flow rates can be computed from the unit volume of blood and the inner cavity cross-section of silicone microtubule. The section of silicone microtubule illuminated by a focal spot and the focus-typed ultrasonic sensor attached by a plastic cylinder were all placed in a water tank. In the experimental equipment, pure water was filled between the silicone microtubule and the front port of the ultrasonic sensor and used as the coupling gel to obtain a stable optoacoustic signal. To explore the impact of the detection distance, the ultrasonic sensor was connected with the 3D electric platform via a fixed bracket, and then the detection distance could be changed via the 3D electric platform. At the same time, the focal spot can be accurately dropped into the blood sample in the silicone microtubule by adjusting the 3D electric platform. To explore the impact of temperature, a temperature controller with a magnetic stirring function (SN-MS-H280D, SUNNE Co., China) was adopted in this work. The temperature controller has the function of heating and constant temperature, which can heat and control the temperature of blood samples. Moreover, to ensure the uniform heating of the blood sample and to avoid coagulation, a magnetic rotor was placed into the beaker to automatically stir the blood sample. At the same time, a temperature sensor was utilized to get the temperature of blood sample. For the influence of energy absorption, the excitation energy of laser can be adjusted via the laser control software. In experiments, to obtain the actual BGVs of blood samples, a blood glucose metre (GA-3, Sinocare Co., China) and test strips were utilized. Before the experiments, the OPO pulse laser and other electronic devices were preheated for approximately 30 min, and the ambient temperature was controlled at 20 ± 0.5 °C.

3.2. Material and configurations

A total of 625 rabbit whole blood samples were utilized as the experimental samples in the experiments. Rabbit whole blood was purchased from Zhengzhou Yikang Bioengineering Co., Ltd. To avoid blood clotting, 1.6 mg/ml ethylenediaminetetraacetic acid (EDTA) anticoagulant was added to rabbit whole blood. Fig. 3(b) gives experimental blood.

To investigate the synthetic impact of several variables (temperature, BGV, energy absorption, flow rate and detection distance) on the optoacoustic measurement of DM, the reasonable values are configured for each influence variable, which are given in Table 1. For BGV, five values of BGV correspond to five different degrees of DM in clinics, i.e., hypoglycaemia, normal, slight diabetes, moderate diabetes and severe diabetes, respectively.

3.3. Results and analysis

According to the constructed optoacoustic experimental equipment of blood glucose, the optoacoustic signals of 625 cases of blood samples with the combinations of impacting variables were acquired. Due to space limitations, only part of the optoacoustic signals for different BGVs are presented in Fig. 4(a)-(d).

As shown in Fig. 4, the profiles of the optoacoustic signal of blood glucose under different impacting combinations are roughly the same, but the amplitudes are different. In Fig. 4(a), when the energy absorption, temperature, flow rate and detection distance are fixed, with increasing BGV, the amplitude of the optoacoustic signal increases. In Fig. 4(b), when the values of other impacting variables are fixed, with increasing temperature, the optoacoustic amplitude increases. In Fig. 4(c), although the time of the first peak for the optoacoustic signals increases with the detection distance, the amplitude of the optoacoustic signals increases with the energy absorption. Fig. 4(d) presents with the increase of flow rate, the amplitude of optoacoustic signals decreases. Therefore, under the synthetic impact of several variables, the change in optoacoustic intensity of blood glucose is complicated. The factors that induce an increase in the optoacoustic intensity of blood glucose include not only the BGV but also the temperature and energy absorption. Conversely, the detection distance and flow rate are the factors that induce a decrease in the optoacoustic intensity of blood glucose. Moreover, in Fig. 4, the aliasing phenomenon of the optoacoustic signal under different BGVs is strong, which makes classifying blood samples with different BGVs difficult. To avoid the complicacy of the classification model due to the large characteristic dimension of blood samples, optoacoustic peak–peak values with different combinations of several variables were acquired and shown in Fig. 5.

In Fig. 5(a) and (b), although optoacoustic peak–peak values increase with BGV, energy absorption and temperature are also important positive variables. According to Fig. 5(c) and (d), the BGV isn't easy to be classified because the peak-peak value differences under the different flow rates and detection distances are little. Moreover, in Fig. 5(a)–(d), with the synthetic impacts of several variables, the optoacoustic peak–peak values are aliased, which is not favourable for qualitatively classifying the BGV. To make an

Table 1
Configurations of five influence variables.

Temperature/°C	BGV/mmol/L	Energy absorption/mJ	Flow rate/m/s	Detection distance/mm
36	2	0.15	0.057	12
37	5	0.26	0.099	13
38	8	0.37	0.145	14
39	11	0.49	0.184	15
40	14	0.62	0.219	16
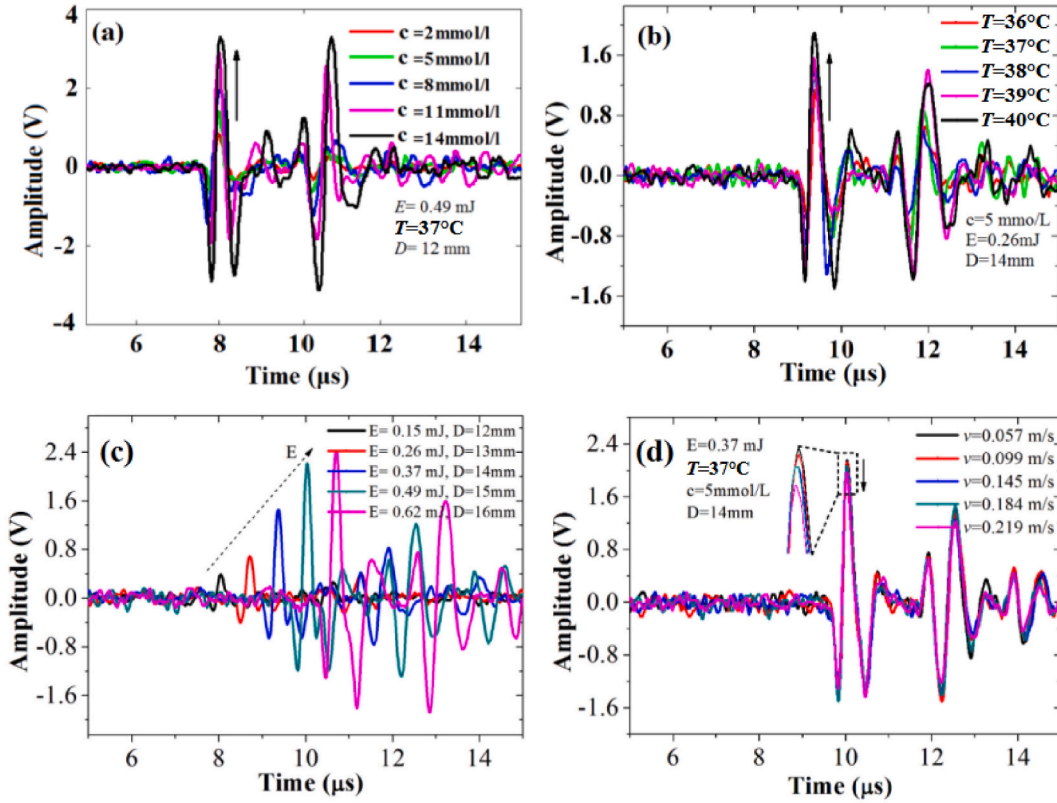
Fig. 4. Optoacoustic signals of blood samples at different impacting combinations. (a) different BGVs; (b) different temperatures; (c) different energy absorption and detection distances; and (d) different flow rates.

accurate qualitative classification of BGVs, an artificial intelligence (AI) method was utilized to classify the DM with the synthetic impacts of several variables in this study.

4. Qualitative classification

4.1. Classification results

Firstly, WNN algorithm was utilized to classify BGV of DM with the synthetic impacts of several variables based on optoacoustic peak–peak values for rabbit whole blood samples.

For 625 cases of rabbit whole blood samples, training and testing samples were randomly allocated at 4:1 ratio. Then, energy absorption, temperature, flow rate, detection distance and peak–peak values were set as input variable of WNN. All BGVs were labeled as 1 to 5 according to five different degrees of DM, i.e., hypoglycaemia was labeled with Category 1, normal was labeled with Category 2, slight diabetes was labeled with Category 3, moderate diabetes was labeled with Category 4, and severe diabetes was labeled with Category 5. Then, to enhance the qualitative classification accuracy of BGVs, the PSO was utilized to optimize weight values of WNN, as well as scaling and translation variables of wavelet activation function. Additionally, parameters of WNN structure should be optimized, i.e., the number of neurons in hidden layer (k) and two learning rates (η, λ).

To obtain the value of k, Eq. (11) [59] was employed:

$$k = \sqrt{p+j} + \vartheta \tag{11}$$

In Eq. (11), p and j denotes the neurons in input and output layers. In this work, p and j are both 5. ϑ is a constant ranging from [0, 10]. Based on Eq. (11), $k \in [3, 13]$.

For the optimal solution search of PSO, the particles' speed $s(m)$ and position $p(m)$ are the crucial parameters that should be renewed by means of Eq. (12):

$$\begin{cases} s^i(m+1) = \omega \cdot s^i(m) + c_1 \cdot rad_1 \cdot \left(P^i - p^i(m)\right) + c_2 \cdot rad_2 \cdot \left(G^i - p^i(m)\right) \\ p^i(m+1) = p^i(m) + s^i(m+1) \end{cases} \tag{12}$$

where $s^i(m)$ and $s^i(m+1)$ the original and renewed velocities, respectively. ω ($\omega \in [0, 1]$) denotes the inertia weight. $p^i(m)$ and $p^i(m+1)$
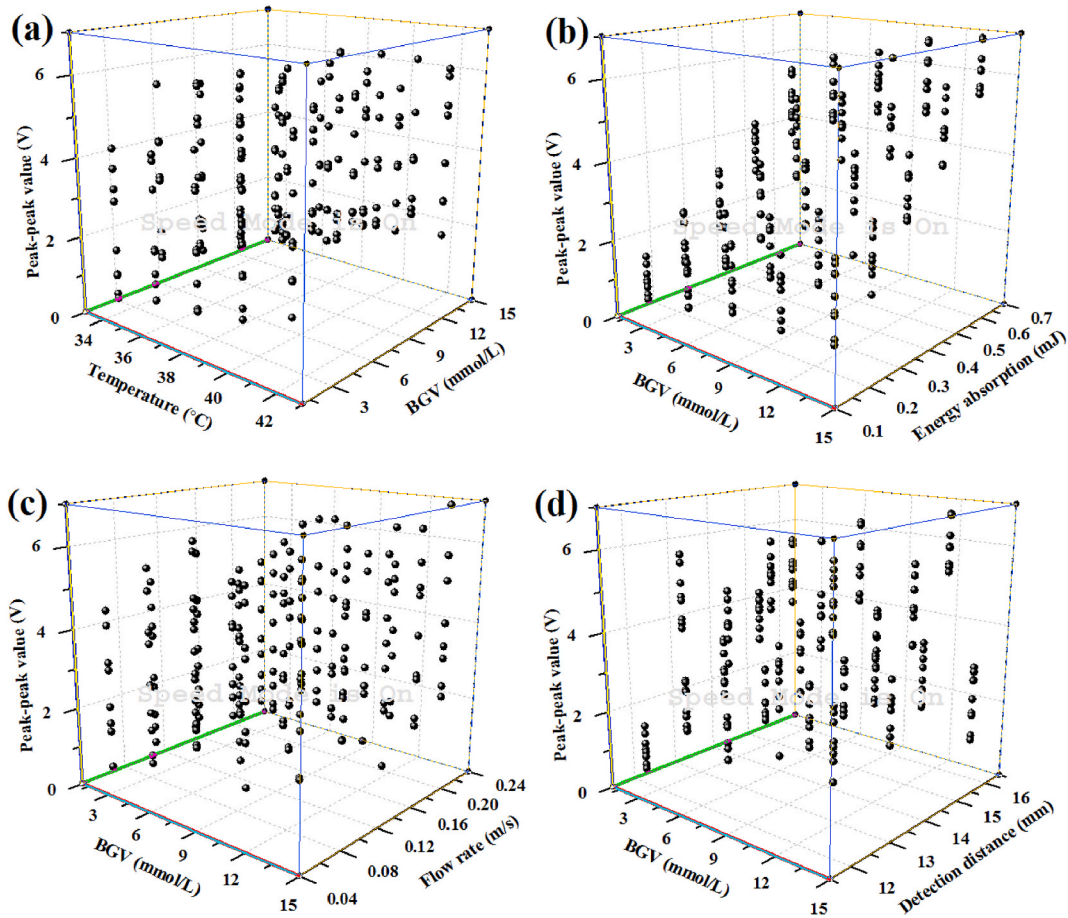
Fig. 5. 3D distributions of optoacoustic peak–peak values of blood samples under the synthetic impacts of several variables under temperatures and BGVs (a), under the BGVs and energy absorption (b), under the BGVs and flow rates (c), and under the BGVs and detection distances (d).

denote the original and renewed positions, respectively. c_1 and c_2 denote two accelerated variables, and rad_1, rad_2 are the random numbers, i.e., $rad_1, rad_2 \in (0,1)$. P^i and G^i denote the local and global optimal particle directions.

To determine the optimal values of k, η and λ, the influences of k, η and λ on the classification accuracy of BGV were all researched, as presented in Fig. 6(a)-(c).

In Fig. 6(a), with the synthetic impacts of several variables, for the WNN, when $k = 13$, the highest classification accuracy of BGV can reach 65.6 %. However, for PSO-WNN, when $k = 6$, the highest classification accuracy of BGV can reach 92.8 %. Moreover, the classification accuracies of BGV for PSO-WNN are higher under all neuron numbers. In addition, to find the optimal η in [0.001, 0.01] for both algorithms, Fig. 6(b) presents the impact of η on classification accuracy. In Fig. 6(b), for WNN, when $\eta = 0.01$, the classification accuracy of BGV was the highest, improving from 65.6 % to 88.8 %. For PSO-WNN, when $\eta = 0.008$, the classification accuracy of BGV was the highest, improving from 92.8 % to 96 %. Moreover, the classification accuracies of BGV for PSO-WNN are higher under all η values. Then, to get the optimal λ from [0.01, 0.1] for both algorithms, Fig. 6(c) gives the influences of λ on the classification accuracy. In Fig. 6(c), for WNN, when $\lambda = 0.01$, the classification accuracy of BGV was the highest, increasing from 88.8 % to 94.4 %. However, for PSO-WNN, when $\lambda = 0.02$, the classification accuracy of BGV was the highest, increasing from 96 % to 98.4 %. Moreover, the classification accuracies of PSO-WNN were also higher under all λ values. According to Fig. 6(a), (b) and (c), classification performance of PSO-WNN exceeds WNN.

To study the effect of PSO-WNN on classification accuracy of BGV with the synthetic impacts of several variables, three parameters in the PSO-WNN algorithm were optimized, i.e., inertia weight (w) and two accelerated variables (c_1 and c_2) in Eqs.(12). To get the optimal three aforementioned parameters of PSO-WNN, the impacts of inertial weight (w) and accelerated variables (c_1 and c_2) on classification accuracy of BGV were obtained, as given in Fig. 7(a)–(e).

As can be seen from Eqs.(12), the accelerated variables (c_1 and c_2) jointly affect the motion speed of particles in PSO. For larger c_1, the local searching capacity becomes better but the global searching capacity becomes poor, so that particles are easy to drop in the local optima, and the optimum's searching rate is reduced. On the contrary, for the larger c_2, the situation is just opposite to that of c_1, and affects the selection of optimal particle.

To better get the optimal c_1 and c_2, according to past experience [60], the accelerated variable c_2 was configured as 2, and w was
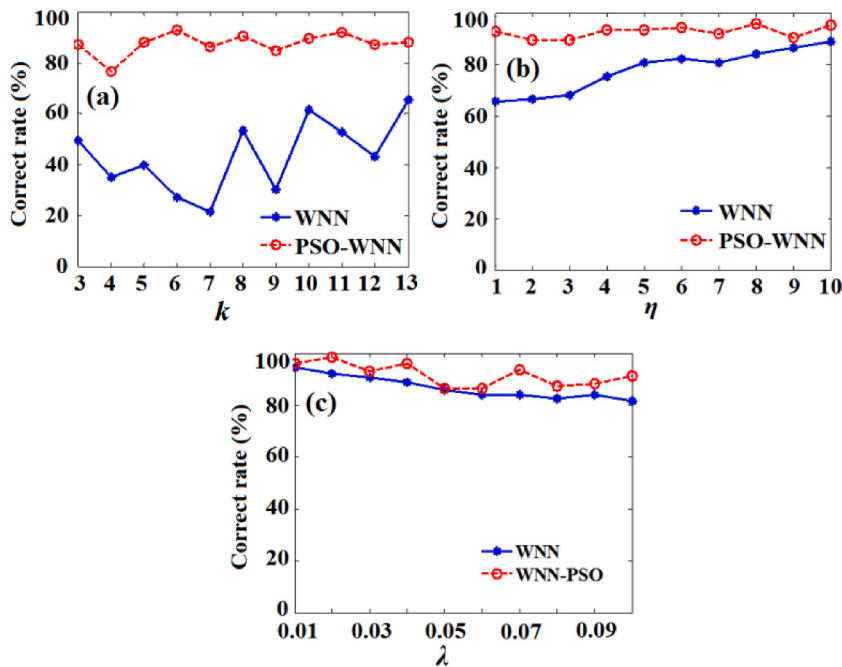
Fig. 6. Influences of k (a), η (b) and λ (c) on the classification accuracy of BGV.

selected as 0.6 to obtain the optimal c_1 from Refs. [1,2]. In Fig. 7(a), the optimal value of accelerated variable c_1 is 2 because the highest classification accuracy reaches 98.4 %. Then, the influence of accelerated variable c_2 on the classification accuracy of the BGV was studied under $c_1 = 2$ and $w = 0.6$. As shown in Fig. 7(b), when $c_2 = 1.9$ and 2, the classification accuracy was highest. Then, to get the optimal accelerated variable c_2, the convergent rates under $c_2 = 1.9$ and 2 were compared and are presented in Fig. 7(c). The convergent rate $c_2 = 2$ is obviously faster than $c_2 = 1.9$. Therefore, $c_2 = 2$ is the optimal accelerated variable c_2. Finally, the influence of w on classification accuracy of BGV was investigated under $c_1 = 2$ and $c_2 = 2$, as given in Fig. 7(d). In Fig. 7(d), when $w = 0.5, 0.6, 0.9$ and 1, the classification accuracy was highest. To further determine the optimal inertia weight w, the convergence speeds under $w = 0.5, 0.6, 0.9$ and 1 were compared and are presented in Fig. 7(e). In Fig. 7(e), $w = 1$ is optimal because the convergent rate of $w = 1$ is fastest. Therefore, a set of optimal parameters of the PSO-WNN algorithm were determined to be $c_1 = c_2 = 2$ and $w = 1$.

Finally, the influence of iteration number on the classification accuracy of BGV, the influence of training number on mean-square-error (MSE) of BGV were investigated, which are presented in Fig. 8(a) and (b). Fig. 8(c) gives the classification results of testing blood under the optimal parameters.

As shown in Fig. 8(a), for the number of iteration is 1, classification accuracy of BGV based on PSO-WNN is 69.6 %, lower than WNN. As the number of iteration increases, classification accuracy of BGV gradually increases. When the iteration number increases to 7, the classification accuracy of the BGV for PSO-WNN increases from 69.6 % to 98.4 %, which exceeds the classification accuracy of the BGV based on the WNN. As the iteration number continuously increases, the classification accuracy reaches 98.4 %.

Fig. 8(b) presents the impact of the number of training on MSE of BGV. With increasing training number, the MSE curves of BGV for the WNN and PSO-WNN all decrease continuously. Moreover, MSE of PSO-WNN are larger than WNN.

Under these determined optimal variables of WNN and PSO-WNN, the categories corresponding to 125 testing samples were classified, and the testing results based on both algorithms are presented in Fig. 8(c). The classification accuracy of BGV based on WNN is 94.4 % for 125 groups of testing blood. Seven samples were incorrectly classified, i.e., the misjudgment rate was 5.6 %, among which one normal sample (Category 2) was misjudged as slight diabetes (Category 3), one sample with slight diabetes (Category 3) was misjudged as moderate diabetes (Category 4), and four samples with moderate diabetes (Category 4) were misjudged as slight diabetes (Category 3). One sample with moderate diabetes (Category 4) was misjudged as severe diabetes (Category 5). For the PSO-WNN, the classification accuracy of 125 testing blood reached 98.4 %, and only two samples were incorrectly classified, i.e., the misjudgment rate was 1.6 %, among which one normal sample (Category 2) was misjudged as moderate diabetes (Category 4) and one sample with slight diabetes (Category 3) was misjudged as moderate diabetes (Category 4).

4.2. Classification results of BGV for QPSO-WNN

To further enhance classification accuracy of BGV with the synthetic impacts of several variables, QPSO was utilize to optimize WNN, i.e., QPSO-WNN. As same as PSO-WNN, k, η and λ of QPSO-WNN should also be adjusted. For QPSO-WNN algorithm, the influences of k, η and λ on classification accuracy of BGVs with synthetic impact of several variables were presented in Fig. 9(a)-(e).

In Fig. 9(a), when k of QPSO-WNN is 12 or 13, classification accuracy of BGV can reach 93.6 %. The classification accuracies of BGV
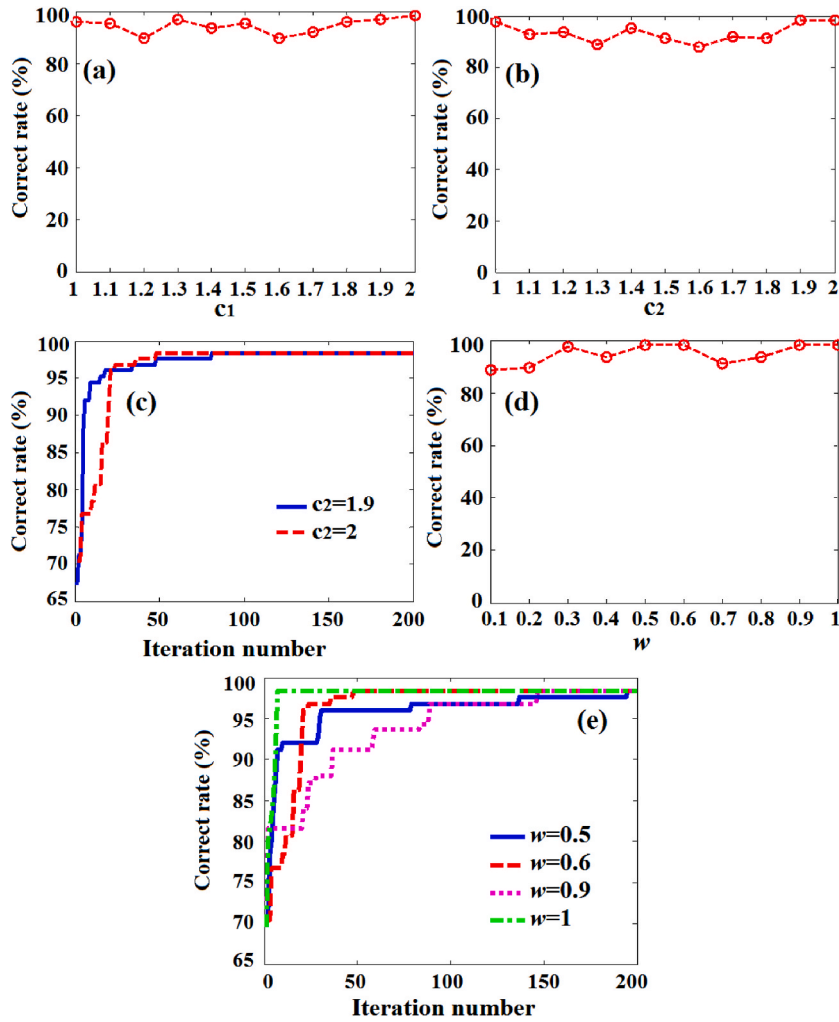
Fig. 7. Effect of parameters of PSO-WNN on classification accuracy of BGV with the synthetic impacts of several variables. (a) accelerated variable c_1; (b) accelerated variable c_2; (c) optimal selection of accelerated variable c_2; (d) inertia weight w; (e) optimal selection of inertia weight w.

under all values of k are greater than PSO-WNN and WNN. To get the optimal k of QPSO-WNN, the convergent rates for $k = 12$ and 13 were compared and are presented in Fig. 9(b). The convergent rate of $k = 12$ is faster than that of 13. Therefore, the optimal value of k for QPSO-WNN is 12.

In addition, the optimal η of QPSO-WNN should be determined, and classification accuracy of BGV was enhanced with the synthetic impact of several variables. Fig. 9(c) presents the impact of η on classification accuracy of BGV for QPSO-WNN. In the range of $\eta =$ [0.001, 0.01] for the QPSO-WNN algorithm, when $\eta = 0.009$ and 0.01, the classification accuracies of BGV were highest, increasing from 93.6 % to 98.4 %. Moreover, the classification accuracies of BGV for all η values of QPSO-WNN were higher. To obtain the optimal η, convergent rates of $\eta = 0.009$ and 0.01 were compared and presented in Fig. 9(d). The convergent rate of $\eta = 0.01$ is faster than $\eta =$ 0.009. Therefore, $\eta = 0.01$ is the optimal learning rate. Fig. 9(e) shows the influence of λ on classification accuracy of BGV for QPSO-WNN. In the range of $\lambda =$ [0.01, 0.1] for the QPSO-WNN algorithm, when $\lambda = 0.01$, the classification accuracy of BGV was the highest, increasing from 98.4 % to 100 %. Similar to that of η, the classification accuracies of all λ values were higher than WNN and PSO-WNN.

Then, the shrinkage and expansion coefficient (α) of QPSO-WNN was optimized in the range of [0.1, 1]. To determine the optimal shrinkage and expansion coefficient α, the influence of shrinkage and expansion coefficient α on the classification accuracy of BGV for QPSO-WNN was presented in Fig. 10(a)-(b).

As shown in Fig. 10(a), when $\alpha = 0.3, 0.5, 0.6, 0.7, 0.8$ and 1, the classification accuracies of BGV were largest for the QPSO-WNN algorithm. To further determine the optimal shrinkage and expansion coefficient, Fig. 10(b) shows the relationships between the iteration number and the classification accuracy for $\alpha = 0.3, 0.5, 0.6, 0.7, 0.8$ and 1. According to Fig. 10(b), the convergent rate of $\alpha =$ 0.3 was the fastest, demonstrating that the optimal shrinkage and expansion coefficient α is 0.3.

Finally, the influence of iteration number on the classification accuracy of BGV, the influence of training number on the MSE, and the classification results of testing blood were studied, as presented in Fig. 11(a)-(c).
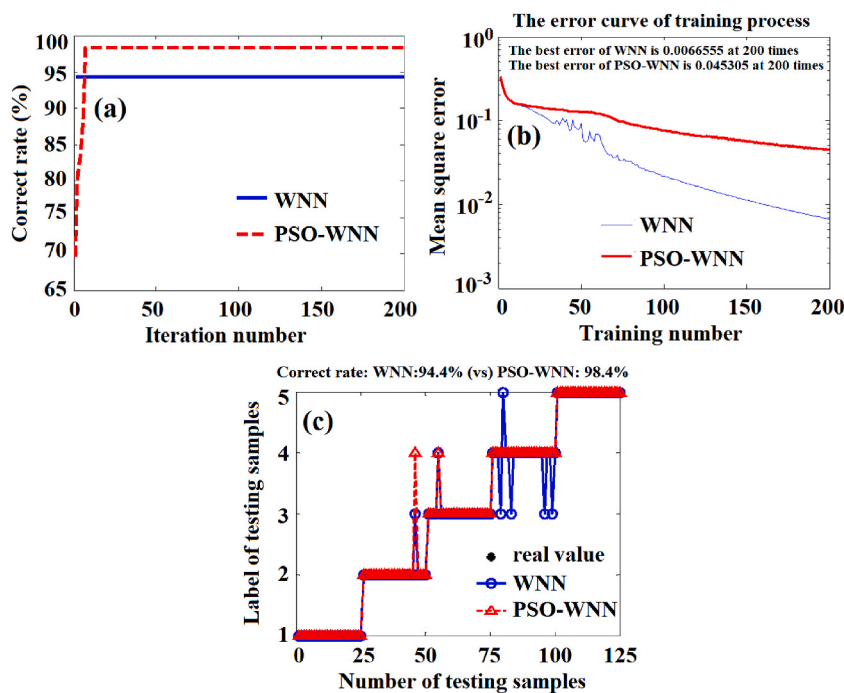
Fig. 8. Comparison of classification accuracy for BGV between WNN and PSO-WNN. (a) influence of iteration number on the classification accuracy; (b) influence of training number on MSE of BGV; (c) classification results of testing blood.

As shown in Fig. 11(a), as the iteration number of 1, the classification accuracy of QPSO-WNN is 93.6 %. As increasing the iteration number, the classification accuracy of BGV gradually increases. When the iteration number increases to 21, the classification accuracy of BGV increases from 93.6 % to 100 %, which exceeds the classification accuracy of the BGV based on WNN and PSO-WNN. With a further increase in the iteration number, the classification accuracy of BGV reaches 100 %. In Fig. 11(b), with increasing training number, the MSE of classifying BGVs decreases exponentially. Based on optimal parameters of QPSO-WNN, 125 cases of testing blood were predicted, as presented in Fig. 11(c). The classification accuracy of the BGV based on QPSO-WNN for 125 cases of testing blood is 100 %, that is, all testing set samples were correctly classified.

5. Discussion

5.1. Analysis of impacting variables

The accurate measurement and classification of BGV is one of most important steps during the monitoring and controlling of DM. Although optoacoustic spectroscopy has unique advantages based on the effect of opto-induced ultrasonic, which can overcome the interference of scattering light and the problems of spectral overlap and low detection depth for pure optical methods in biotissue, it will inevitably be simultaneously impacted by some elements in practice, especially for changeable circumstances and complicated biobodies. Therefore, to obtain an accurate qualitative assessment or quantitative measurement of BGV for DM patients in the clinic, it is necessary and valuable to explore the impacting of some variables on the optoacoustic measurement of DM and the qualitative classification of its severity.

Although the optoacoustic measurement of blood glucose has already been studied by some scholars and a few reports about the influence of a single variable mainly focused on the temperature and concentration, research on the synthetic impacts of several variables on the optoacoustic measurement of blood glucose has been scarce. For the influence of single variable, its influence patterns is usually obvious. For example, regarding temperature, the optoacoustic intensity of blood glucose linearly increases with temperature [32,33]. For the excitation energy of the laser, its influence pattern is the same as that of the temperature, and the optoacoustic intensity linearly increases with laser's excitation energy [61]. For the detection distance, its influence pattern is opposite to that of temperature and the excitation energy of the laser; that is, the optoacoustic intensity linearly decreases with detection distance. For the BGV, although the relationship between optoacoustic intensity and BGV was built via linear model in some literature [21,22,61], its influence pattern is relatively complicated because the BGV change will cause different changes in other properties of the blood, including mechanical, optical and thermal. In some results, nonlinear modelling between the BGV and the optoacoustic value was used [23,62]. Moreover, from Eq. (1), the optoacoustic intensity is related to many variables. The ultrasonic velocity, optical absorbance coefficient and coefficient of thermal expansion are positively dependent on the optoacoustic intensity. The specific heat volume is negatively dependent on the optoacoustic intensity. In addition, from the experimental results for the impacts of several variables on
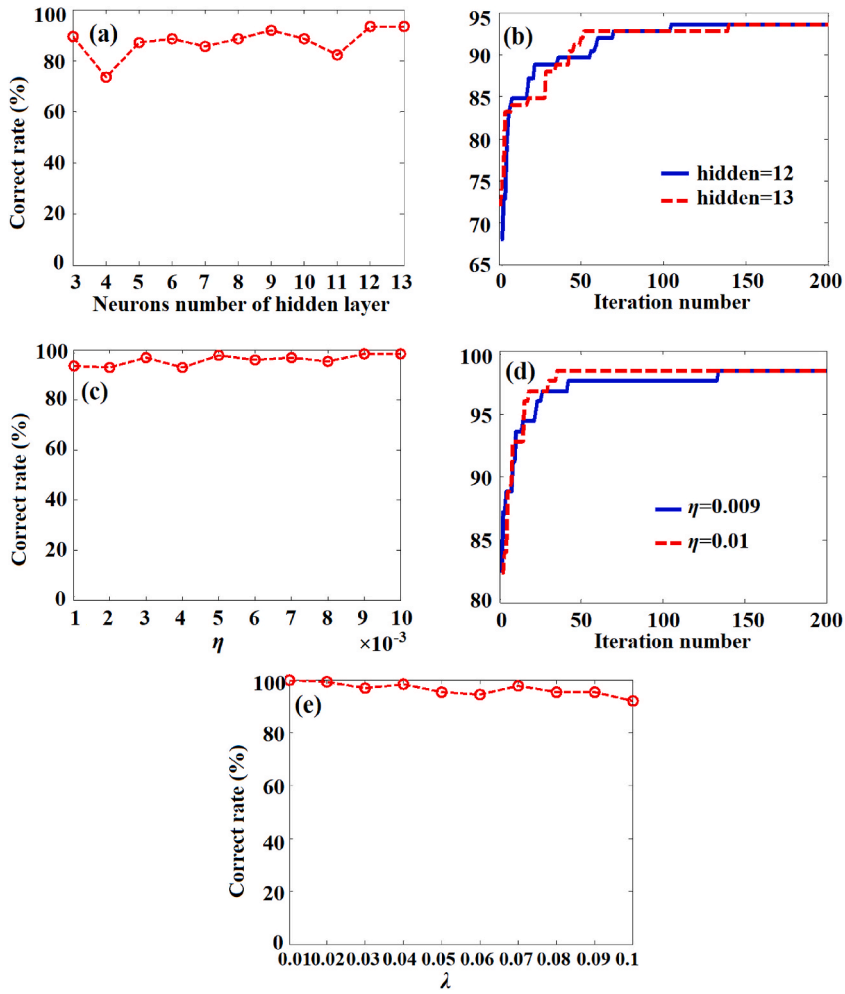
Fig. 9. Influence of the parameters of QPSO-WNN algorithm on the classification accuracy of BGVs with the synthetic impacts of several variables. (a) k; (b) optimal selection of k; (c) η; (d) optimal selection of η; (e) λ.
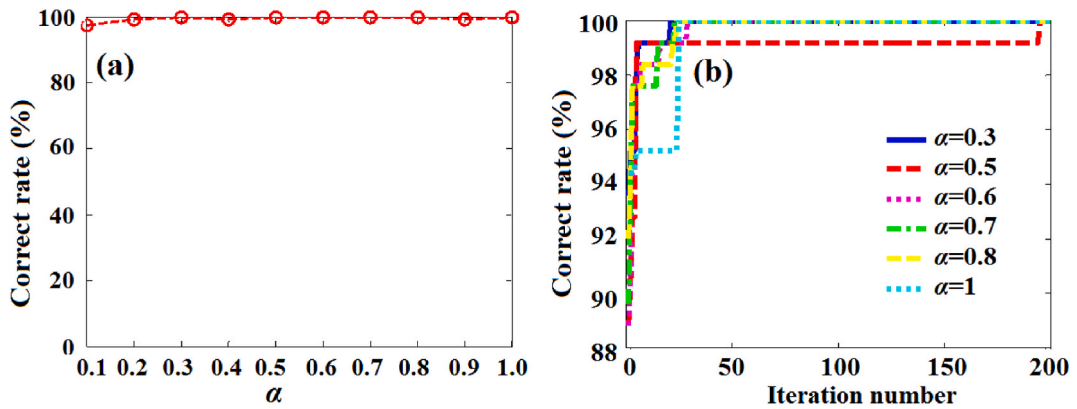
Fig. 10. Effects of the parameters for QPSO-WNN on the classification accuracies of BGVs with synthetic impacts of several variables. (a) effect of shrinkage and expansion coefficient; (b) optimal selection of shrinkage and expansion coefficient.

the optoacoustic measurement of blood glucose in this work (see Fig. 5 in Section 3.3), the reasons for the increase in the optoacoustic intensity (peak–peak values) of blood glucose are not only the BGV but also the excitation energy of the laser and temperature. At the same time, the variables that decrease the optoacoustic intensity of blood glucose are detection distance and flow velocity. Therefore,
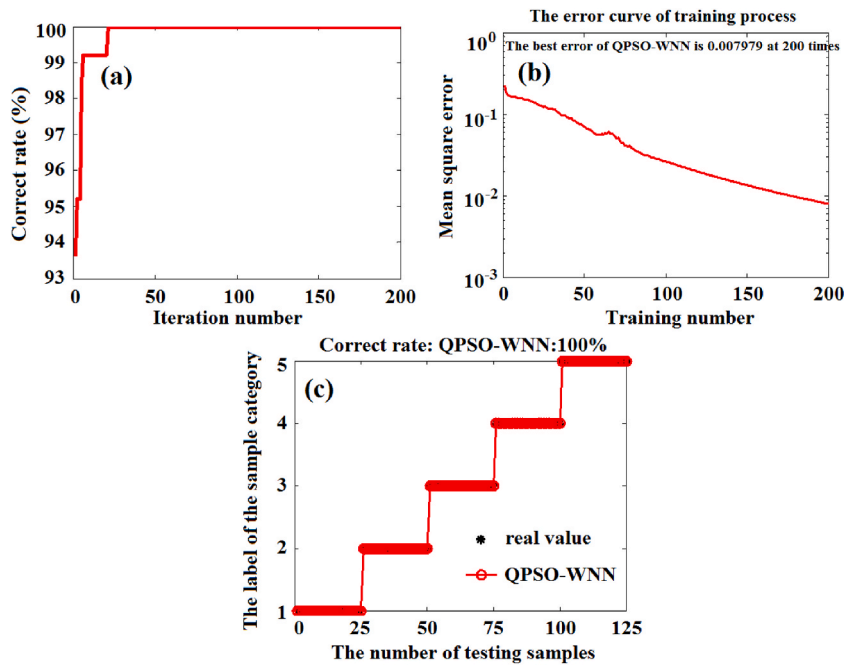
Fig. 11. Classification results of BGV based on QPSO-WNN. (a) the influence of iteration number on the classification accuracy; (b) the influence of training number on MSE; (c) the classification results of testing samples.

with the synthetic impacts of several variables, the change in optoacoustic intensity of blood glucose is usually nonlinear and very complicated. It is difficult to rapidly and accurately classify the different severities of DM from only complicated and changeable real-time optoacoustic signals or optoacoustic intensity. Therefore, it is necessary to use machine learning [63–66] or artificial intelligence methods [67,68] to analyse the optoacoustic data of blood glucose and then to accurately achieve the qualitative classification of DM with different BGVs. In this work, the qualitative classification of DM with the synthetic impacts of several variables was first studied via optoacoustic technology. Moreover, the WNN algorithm was utilized to develop the qualitative classification model for the DM severity. At the same time, the PSO and QPSO algorithms were utilized to optimize the variables of WNN. For the PSO, too many variables should be adjusted in *Eqs.* (12), that is, not only positions and velocities of particles need to be updated but also three control parameters need to be adjusted, that is, inertia weight (w), accelerated variable (c_1) and accelerated variable (c_2). However, for the QPSO, only the positions of particle need to be updated in *Eqs.* (7), and there is only one control parameter, i.e., shrinkage and expansion coefficient.

5.2. Comparison and validation

To validate the availability of classifying DM based on QPSO-WNN algorithm, the classification results of DM with the synthetic impacts of several variables were compared with seven different algorithms in this work, i.e., extreme learning machine (ELM) [69], SVM [70], self-organizing competitive neutral networks (SOCNN) [71], self-organizing mapping neural networks (SOMNN) [72], WNN, PSO-WNN and QPSO-WNN. Table 2 shows the classification accuracies of BGV based on seven algorithms.

In Table 2, the classification accuracies of BGV based on the SOCNN and SOMNN are only 19.2 % and 16.8 %, respectively. The reason why the classification accuracies of BGV based on the SOCNN and SOMNN are not high is that the differences between the optoacoustic peak–peak values for blood glucose samples with different concentrations were very small, which results in the unsatisfactory qualitative classification of BGV from similar data. The classification accuracies of BGV based on ELM and SVM can reach 93.6 % and 92.8 %, respectively, which are much higher than SOCNN and SOMNN. The classification accuracy of BGV based on the WNN can reach 94.4 %, which is slightly higher than ELM and SVM. For WNN, PSO was utilized to optimize the weight values, scaling and translation variables of wavelet activation function in the WNN, and classification accuracy was enhanced from 94.4 % to 98.4 %. Finally, the classification accuracy was further enhanced from 98.4 % to 100 % under the QPSO-WNN. Study results show that the QPSO-WNN has a significant classification result of qualitatively classifying the BGV with the synthetic impacts of multiple variables.

Table 2
The classification accuracies of BGV of DM based on seven algorithms.

Algorithms	SOCNN	SOMNN	ELM	SVM	WNN	PSO-WNN	QPSO-WNN
Accuracy(%)	19.2	16.8	93.6	92.8	94.4	98.4	100

5.3. Prospects

According to the results of this work, optoacoustic technology combined with AI algorithms, such as machine learning (ML) algorithms and ANN algorithms, performs well in the qualitative classification and assessment of DMs involved in synthetic impacts. As this work is the first investigation on the optoacoustic qualitative classification of DM considering the synthetic impacts of five factors, the qualitative classification results of DM are satisfactory, supporting further research on more factors. Research on the optoacoustic qualitative classification and assessment of DM impacted by more complicated influencing variables will be reported in our next work. At the same time, with the optimized design and miniaturization of optoacoustic detection systems, such as pulsed lasers, ultrasonic transducers, signal preprocessing devices, signal acquisition devices, data transfer circuits, data control and microprocessors, the cost performance of optoacoustic detection systems will be greatly improved, which would allow it to enter commercialization and practical application. Therefore, our work has practical research value and can provide strong technical support for future commercial practical applications because it is closer to real-life complicated situations. It is believed that the commercialization of optoacoustic detection and qualitative assessment of DM will be achieved in the near future.

6. Conclusions

Rapid and precise qualitative classification of BGV is very important in assessment of different severities of DM. In this work, an experimental equipment of blood glucose optoacoustic measurement for rabbit whole blood involving the synthetic impacts of several variables was built based on optoacoustic technology. Based on the optoacoustic equipment, we obtained the optoacoustic signals and peak–peak values of blood with different BGVs. As the accurate classification of BGVs is difficult due to the complicated optoacoustic information, WNN algorithm was utilized to qualitatively classify DM with different BGVs in this work. Meanwhile, PSO was utilized to optimize the weight values, scaling and translation variables of wavelet activation function in the WNN. To find some optimal parameters of PSO-WNN, the effects of number of neurons in hidden layer and learning rates on classification accuracy of BGV were investigated. At the same time, the impacts of iteration and training numbers on classification accuracy and MSE of BGV were also studied. Then, QPSO optimized WNN was utilized to further enhance the classification accuracy of BGV. Several conclusions are drawn as follows.

(1) Under the synthetic impacts of several variables, for different BGVs of blood samples, although the optoacoustic signals are very similar in contour, the amplitude increases with increasing temperature, BGV and energy absorption, and decreases with increasing of detection distance and flow rate. In addition, the optoacoustic peak–peak values of blood greatly overlap under the complicated impacts of several variables, which makes classifying the different categories of BGV difficult only from optoacoustic signals or peak–peak values of blood samples.

(2) For WNN algorithm with the optimal number of neurons in hidden layer and learning rates, classification accuracy of DM was 94.4 %. For PSO-WNN algorithm, by adjusting the variables of WNN, as well as PSO, the classification accuracy of DM increased to 98.4 %.

(3) For QPSO-WNN algorithm, by adjusting the number of neurons in hidden layer and learning rates of WNN, the shrinkage and expansion coefficient of QPSO, the classification accuracy of the DM was enhanced to 100 %.

(4) Research results illustrate that optoacoustic technique combined with QPSO-WNN algorithm performs well in the qualitative classification of DM with the synthetic impacts of several variables.

Author contribution statement

Tao Liu: Perform the experiments; Contributed reagents, materials, analysis tools or data; Wrote the paper; Zhong Ren and Shuanggen Huang: Conceived and designed the experiments; Conceptualization and methodology proposal. Chengxin Xiong: Perform the experiments; Analyzed and interpreted the data. Wenping Peng and Junli Wu: Analyzed and interpreted the data. Gaoqiang Liang and Bingheng Sun: Contributed reagents, materials, analysis tools or data.

Funding

Data availability statement

The data presented in this study are available on reasonable request from the corresponding author.

Declaration of competing interest

The authors declare that they have no known competing financial interests or personal relationships that could have appeared to

influence the work reported in this paper.

References

[1] H.M. Wu, C.F. Shi, Q. Zhu, Y. Li, Z.K. Xu, C.J. Wei, D.J. Chen, X.J. Huang, Capillary-driven blood separation and in-situ electrochemical detection based on 3D conductive gradient hollow fiber membrane, Biosens. Bioelectron. 171 (2021), 112722.

[2] R. Yang, Y. Wu, X. Liu, W. Chen, GACSNet: a lightweight network for the noninvasive blood glucose detection, Appl. Artif. Intell. 36 (2022), 2081898.

[3] B.G. Pedro, D.W.C. Marcôndes, P. Bertemes-Filho, Analytical model for blood glucose detection using electrical impedance spectroscopy, Sensors-Basel 20 (2020) 6928.

[4] D. Bruen, C. Delaney, L. Florea, D. Diamond, Glucose sensing for diabetes monitoring: recent developments, Sensors 17 (2017) 1866.

[5] J. Yadav, A. Rani, V. Singh, B.M. Murari, Prospects and limitations of non-invasive blood glucose monitoring using near-infrared spectroscopy, Biomed. Signal Proces. 18 (2015) 214–227.

[6] G. Han, S.Q. Chen, X.Y. Wang, J.H. Wang, H.Q. Wang, Z. Zhao, Noninvasive blood glucose sensing by near-infrared spectroscopy based on PLSR combines SAE deep neural network approach, Infrared Phys. Techn. 113 (2021), 103620.

[7] T.L. Chen, Y.L. Lo, C.C. Liao, Q.H. Phan, Noninvasive measurement of glucose concentration on human fingertip by optical coherence tomography, J. Biomed. Opt. 23 (2018), 047001.

[8] S. Amrane, N. Azami, Y. Elboulqe, Mixed integer non linear algorithm for dermis detection for glucose blood monitoring based on optical coherence tomography, Inter. J. Appl. Eng. Research 11 (2016) 7151–7154.

[9] E.A. Shirshin, O.P. Cherkasova, T. Tikhonova, E. Berlovskaya, A.V. Priezzhev, V. Fadeev, Native fluorescence spectroscopy of blood plasma of rats with experimental diabetes: identifying fingerprints of glucose-related metabolic pathways, J. Biomed. Opt. 20 (2015), 051033.

[10] R. Ballerstadt, C. Evans, A. Gowda, R. McNichols, In vivo performance evaluation of a transdermal near-infrared fluorescence resonance energy transfer affinity sensor for continuous glucose monitoring, Diabetes Technol. The. 8 (2006) 296.

[11] Z.F. Yu, Q. Qiu, Y. Guo, Dual modulation optical polarimetry for glucose monitoring, Acta Opt. Sin. 36 (2016), 0117001.

[12] X. Yang, A.Y. Zhang, D.A. Wheeler, T.C. Bond, C. Gu, Y. Li, Direct molecule-specific glucose detection by Raman spectroscopy based on photonic crystal fiber, Anal. Bioanal. Chem. 402 (2012) 687–691.

[13] J.W. Kang, Y.S. Park, H. Chang, W. Lee, S.P. Singh, W. Choi, L.H. Galindo, R.R. Dasari, S. Nam, J. Park, P.T.C. So, Direct observation of glucose fingerprint using in vivo Raman spectroscopy, Sci. Adv. 6 (2020), eaay5206.

[14] S.D. Russo, A. Sampaolo, P. Patimisco, G. Menduni, M. Giglio, C. Hoelzl, V.M.N. Passaro, H. Wu, L. Dong, V. Spagnolo, Quartz-enhanced photoacoustic spectroscopy exploiting low-frequency tuning forks as a tool to measure the vibrational relaxation rate in gas species, Photoacoustics 21 (2021), 100227.

[15] J.Y. Sim, C.G. Ahn, E.J. Jeong, B.K. Kim, In vivo microscopic photoacoustic spectroscopy for non-invasive glucose monitoring invulnerable to skin secretion products, Sci. Rep.-UK 8 (2018) 1059.

[16] T. Tajima, Y. Okabe, Y. Tanaka, M. Seyama, Linearization technique for dual-wavelength CW photoacoustic detection of glucose, IEEE Sens. J. 17 (2017) 5079–5086.

[17] S. El-Busaidy, B. Baumann, M. Wolff, L. Duggen, H. Bruhns, Experimental and numerical investigation of a photoacoustic resonator for solid samples: towards a non-invasive glucose sensor, Sensors-Basel 19 (2019) 2889.

[18] Y. Tanaka, T. Tajima, M. Seyama, Acoustic modal analysis of resonant photoacoustic spectroscopy with dual-wavelength differential detection for noninvasive glucose monitoring, IEEE Sensors Letters 1 (2017) 1–4.

[19] A. Aloraynan, S. Rassel, C. Xu, D.Y. Ban, A single wavelength mid-infrared photoacoustic spectroscopy for noninvasive glucose detection using machine learning, Biosensors-Basel 12 (2022) 166.

[20] T. Namita, M. Sato, K. Kondo, M. Yamakawa, T. Shiina, Evaluation of Blood Glucose Concentration Measurement Using Photoacoustic Spectroscopy in Near-Infrared Region. Proc. SPIE, vol. 10064, Photons Plus Ultrasound: Imaging and Sensing, 2017, 100645A-1.

[21] R. Zhang, F. Gao, X. Feng, S. Liu, R. Kishor, Y. Luo, Y. Zheng, Noninvasive photoacoustic measurement of glucose by data fusion, Analyst 142 (2017) 1–5.

[22] Y. Shen, Z. Lu, S. Spiers, H.A. MacKenzie, J. Lindberg, Measurement of the optical absorption coefficient of a liquid by use of a time-resolved photoacoustic technique, Appl. Optics 39 (2000) 4007–4012.

[23] Y.J. Zhang, S. Chen, Y.L. Yu, J.H. Wang, A miniaturized photoacoustic device with laptop readout for point-of-care testing of blood glucose, Talanta 209 (2020), 120527.

[24] A. Srivastava, M.K. Chowdhury, S. Sharma, N. Sharma, In-vitro measurement of glucose concentration in human blood plasma mixed intralipid phantom samples by using modulated ultrasound and infrared light, British Biotechnol. J. 13 (2016) 1–14.

[25] W.Y. Tsai, S. Breimann, T.W. Shen, D. Frishman, Photoacoustic and absorption spectroscopy imaging analysis of human blood, PLoS One 18 (2023), e0289704.

[26] H. Long, B. Chen, W. Li, Y. Xian, Z. Peng, Blood glucose detection based on Teager-Kaiser main energy of photoacoustic signal, Comput. Biol. Med. 134 (2021), 104552.

[27] J. Ahn, J.W. Baik, D. Kim, K. Choi, S. Lee, S.M. Park, J.Y. Kim, S.H. Nam, C. Kim, In vivo photoacoustic monitoring of vasoconstriction induced by acute hyperglycemia, Photoacoustics 30 (2023), 100485.

[28] L. Yang, Z. Zhang, X. Wei, Y. Yang, Glucose diagnosis system combining machine learning and NIR photoacoustic multispectral using a low power CW laser, Biomed. Opt Express 14 (2023) 1685–1701.

[29] L. Yang, C. Chen, Z. Zhang, X. Wei, Glucose determination by a single 1535 nm pulsed photoacoustic technique: a multiple calibration for the external factors, J. Healthc. Eng. 2022 (2022) 1–10.

[30] A. Aloraynan, S. Rassel, C. Xu, D. Ban, A single wavelength mid-infrared photoacoustic spectroscopy for noninvasive glucose detection using machine learning, Biosensors 12 (2022) 166.

[31] M.R. Kaysir, J. Song, S. Rassel, A. Aloraynan, D. Ban, Progress and perspectives of mid-infrared photoacoustic spectroscopy for non-invasive glucose detection, Biosensors 13 (2023) 716.

[32] W. Tao, Z. Lu, Q. He, P. Lv, Q. Wang, H. Zhao, Research on the temperature characteristics of the photoacoustic sensor of glucose solution, Sensors 18 (2018) 4323.

[33] Y. Tanaka, T. Tajima, M. Seyama, K. Waki, Resonant photoacoustic spectroscopy for a non-invasive blood glucose monitoring: human interface and temperature correction technology, in: Proc. SPIE 10878, Photons Plus Ultrasound: Imaging and Sensing, 2019, 1087841.

[34] Z. Zhao, R.A. Myllyla, Photoacoustic blood glucose and skin measurement based on optical scattering effect, Saratov Fall Meeting, Optical Technologies in Biophysics and Medicine III. International Society for Optics and Photonics 4707 (2001) 153–157, 2002.

[35] S.W. Zhao, W. Tao, Q.Z. He, H. Zhao, W.W. Cao, A non-invasive photoacoustic and ultrasonic method for the measurement of glucose solution concentration, AIP Adv. 7 (2017), 035313.

[36] T. Liu, Z. Ren, G.D. Liu, C C Zhang, Photoacoustic detection of glucose for the milk-glucose mixed solution, Proc. SPIE 11617 (2020) 13–20.

[37] Z. Ren, G.D. Liu, Effect of salt content on the photoacoustic detection of glucose solutions, Proc. SPIE 11170 (2019) 8–15.

[38] C. Schmid, C. Haug, L. Heinemann, G. Freckmann, System accuracy of blood glucose monitoring systems: impact of use by patients and ambient conditions, Diabetes Technol. The. 15 (2013) 889–896.

[39] P.P. Pai, P.K. Sanki, S. Sarangi, S. Banerjee, Modelling, verification, and calibration of a photoacoustics based continuous non-invasive blood glucose monitoring system, Rev. Sci. Instrum. 86 (2015), 064901.

[40] P.P. Pai, P.K. Sanki, A. De, S. Bhattacharya, S. Banerjee, Regularized Least Squares Regression for Calibration of Photoacoustic Spectroscopy Based Non-invasive Glucose Monitoring System, 2015 IEEE International Ultrasonics Symposium (IUS), IEEE, 2015, pp. 1–4.

[41] S.W. Zhao, W. Tao, Q.Z. He, H. Zhao, H.W. Yang, Glucose solution determination based on liquid photoacoustic resonance, Appl. Optics 56 (2017) 193–199.

[42] Y. Tanak, T. Tajim, M. Seyam, K. Waki, Differential continuous wave photoacoustic spectroscopy for non-invasive glucose monitoring, IEEE Sens. J. 20 (2020) 4453–4458.

[43] M.K. Dasa, C. Markos, J. Janting, O. Bang, Multispectral photoacoustic sensing for accurate glucose monitoring using a supercontinuum laser, J. Opt. Soc. Am. B 36 (2019) A61–A65.

[44] J. Xie, W. Chen, H. Dai, Distributed cooperative learning algorithms using wavelet neural network, Neural Comput. Appl. 9 (2017) 1–15.

[45] Z.Y. Cao, N. Guo, M.H. Li, K.L. Yu, K.Q. Gao, Back propagation neutral network based signal acquisition for Brillouin distributed optical fiber sensors, Opt Express 27 (2019) 4549–4561.

[46] S. Pervaiz, Z. Ul-Qayyum, W.H. Bangyal, L. Gao, J. Ahmad, A systematic literature review on particle swarm optimization techniques for medical diseases detection, Comput. Math. Method. M 2021 (2021), 5990999.

[47] Y. Shi, R.C. Eberhart, Parameter Selection in Particle Swarm Optimization, Springer Berlin Heidelberg, 1998, pp. 591–600.

[48] J. Sun, B. Feng, W.B. Xu, Particle swarm optimization with particles having quantum behavior, in: Proceedings of the 2004 Congress on Evolutionary Computation, IEEE Cat. No.04TH8753), 2004, pp. 325–331.

[49] J. Yao, J. Xia, K.I. Maslov, M. Nasiriavanaki, V. Tsytsarev, A.V. Demchenko, L.V. Wang, Noninvasive photoacoustic computed tomography of mouse brain metabolism in vivo, Neuroimage 64 (2013) 257–266.

[50] G.J. Diebold, T. Sun, Properties of photoacoustic waves in one, two and three dimensions, Acta Acust. United Ac. 80 (1994) 339–351.

[51] C.K.N. Patel, A.C. Tam, Pulsed optoacoustic spectroscopy of condensed matter, Reviews Mod. Phys. 53 (1981) 517–550.

[52] Z. Ren, T. Liu, G. Liu, Classification and identification of real or fake blood based on OPO pulsed laser induced photoacoustic spectroscopy, Spectrosc. Spect. Anal. 41 (2021) 2734–2741.

[53] P. Ong, Z. Zainuddin, Optimizing wavelet neural networks using modified cuckoo search for multi-step ahead chaotic time series prediction, Appl. Soft Comput. 80 (2019) 374–386.

[54] K. Nisar, Z. Sabir, M. Raja, A.A.A. Ibrahim, D.B. Rawat, Design of morlet wavelet neural network for solving a class of singular pantograph nonlinear differential models, IEEE Access 9 (2021) 77845–77862.

[55] E.H. Houssein, A.G. Gad, K. Hussain, P.N. Suganthan, Major advances in particle swarm optimization: theory, analysis, and application, Swarm Evol. Comput. 63 (2021), 100868.

[56] J. Sun, W. Fang, X. Wu, V. Palade, W. Xu, Quantum-behaved particle swarm optimization: analysis of individual particle behavior and parameter selection, Evol. Comput. 20 (2011) 349–393.

[57] W. Fang, J. Sun, Y. Ding, X. Wu, W. Xu, A review of quantum-behaved particle swarm optimization, IETE Tech. Rev. 27 (2010) 336–348.

[58] J. Sun, X.J. Wu, W. Fang, C.H. Lai, W. Xu, Convergence analysis and improvements of quantum-behaved particle swarm optimization, Inf. Sci. 193 (2012) 81–103.

[59] X. Geng, S. Lu, M. Jiang, Q. Sui, S. Lv, H. Xiao, Y. Jia, L. Jia, Research on FBG-based CFRP structural damage identification using BP neural network, Photonic Sens 8 (2018) 168–175.

[60] C. Ren, N. An, J. Wang, L. Li, B. Hu, D. Shang, Optimal parameters selection for BP neural network based on particle swarm optimization: a case study of wind speed forecasting, Knowl-based Syst. 56 (2014) 226–239.

[61] Z. Ren, G. Liu, Y. Ding, Q. Yao, Studies on the influence factors of the blod glucose photoacoustic measurement based on OPO pulsed laser induction, Spectrosc. Spect. Anal. 38 (2018) 3023–3029.

[62] Z. Ren, G. Liu, Z. Huang, Investigation of glucose concentration measurement based on tunable pulsed laser induced photoacoustic technique, Chin. Opt Lett. 11 (2013), S21701.

[63] M. Habibullah, M. Oninda, A.N. Bahar, A. Dinh, K.A. Wahid, NIR-spectroscopic classification of blood glucose level using machine learning approach, May 5-8, in: IEEE Canadian Conference of Electrical and Computer Engineering, Canada, 2019. Edmonton, AB.

[64] E. Susana, K. Ramli, H. Murfi, N.H. Apriantoro, Non-invasive classification of blood glucose level for early detection diabetes based on photoplethysmography signal, Information 13 (2022) 59.

[65] Z. Li, G. Li, W.J. Yan, L. Lin, Classification of diabetes and measurement of blood glucose concentration noninvasively using near infrared spectroscopy, Infrared Phys.Techn. 67 (2014) 574–582.

[66] A. Rghioui, J. Lloret, L. Parra, S. Sendra, A. Oumnad, Glucose data classification for diabetic patient monitoring, Appl. Sci.-Basel 9 (2019) 4459.

[67] S. Ellahham, Artificial intelligence: the future for diabetes care, Am. J. Med. 133 (2020) 895–900.

[68] H.M. Saraoğlu, F. Temurtas, S. Altıkat, Quantitative classification of HbA1C and blood glucose level for diabetes diagnosis using neural networks, Australas. Phys. Eng. Sci. Med. 36 (2013) 397–403.

[69] G.B. Huang, Q.Y. Zhu, C.K. Siew, Extreme learning machine: theory and applications, Neurocomputing 70 (2006) 489–501.

[70] C. Saunders, M.O. Stitson, J. Weston, L. Bottou, A. Smola, Support Vector Machine-Reference Manual, Technical Report, Department of Computer Science, Royal Holloway, University of London, 1998.

[71] A. Arbi, J. Cao, A. Alsaedi, Improved synchronization analysis of competitive neural networks with time-varying delays, Nonlinear Anal.-Model. 23 (2018) 82–102.

[72] S. Lokesh, K.P. Malarvizhi, D.M. Ramya, P. Parthasarathy, C. Gokulnath, An automatic Tamil speech recognition system by using bidirectional recurrent neural network with self-organizing map, Neural Comput, Appl 31 (2019) 1521–1531.